International Forum on Aeroelasticity and Structural Dynamics
IFASD 2024
17-21 June 2024, The Hague, The Netherlands

APPLICATION OF AEROELASTIC TAILORING FOR CONTROL SURFACE REVERSAL

Evangelos Filippou[1], Jurij Sodja[1], Roeland De Breuker[1]

[1]Delft University of Technology
Kluyverweg 1, 2629HS Delft, The Netherlands
e.filippou@tudelft.nl

Keywords: aeroelasticity, structural dynamics, movables, control surface reversal, maneuver load alleviation

Abstract: This research investigates the application of aeroelastic tailoring to enhance the post-control surface reversal regime on a mid-range aircraft. Conventionally, active Maneuver Load Alleviation (MLA) is achieved through control surface actuation, while passive MLA utilizes structural modifications at the material or layout level to exploit wing wash-out deformation. Previous studies have demonstrated the significance of high control effectiveness in active MLA and the limitations of composite tailoring in passive MLA due to roll control authority constraints which typically result in stiffer wings with moderate mass savings. The aeroelastic optimization framework PROTEUS, developed at TU Delft, is employed to enhance operation in the post-control surface reversal regime. This is done to capitalize on increased control authority and thus promote load alleviation. The approach taken in this study is to identify critical constraints and assess the advantages of this strategy while acknowledging the technology's immaturity, particularly its challenges in maintaining roll control effectiveness in certain flight envelope sectors. The results demonstrate significant mass savings in active MLA within the post-control surface reversal regime compared to conventional active MLA and highlight the substantial impact of the cruise-twist constraint on enhancing this regime.

1 INTRODUCTION

Aviation poses a significant challenge in reducing global carbon emissions, contributing just over 2% of energy-related CO_2 emissions yet being hard to decarbonize. Despite a temporary drop in air travel during COVID-19, demand is expected to surge in the coming decade. While new aircraft designs offer up to 20% efficiency improvements, increasing travel demand continues to overshadow these gains. This escalating demand underscores the critical need for the aerospace industry to innovate in aircraft design and radical mass reduction to enhance energy efficiency and maintain safety standards.

According to Brequet range eq. (1) two of the most prominent strategies for reducing aircraft fuel consumption and emissions, are optimizing the lift-to-drag ratio ($\frac{C_L}{C_D}$) and minimizing the structural weight of the aircraft ($\frac{W_{\text{initial}}}{W_{\text{final}}}$).

$$E = \frac{1}{TSFC}\frac{C_L}{C_D}\ln\left(\frac{W_{\text{initial}}}{W_{\text{final}}}\right) \tag{1}$$

Concerning structural weight reduction, load alleviation techniques have emerged to redistribute loads toward the wing root, preventing non-cruise load cases from dominating the structural

design. A further distinction is made between active and passive load alleviation techniques. In the majority of applications, active load alleviation employs control surfaces to mitigate loads, necessitating a high degree of control effectiveness to redistribute loads and, as a consequence, increases wing stiffness and mass [1]. Conversely, passive load alleviation typically employs a combination of material and structural tailoring, exploiting the wash-out behavior of the wing, which is incompatible with the requirement for adequate roll control authority, thus limiting the potential for mass savings [2, 3].

Active load alleviation has been extensively studied for decades and implemented in both commercial and military aircraft [4]. Traditionally, control surfaces are deployed in response to flight conditions to alleviate aerodynamic loads. Recent advancements include the use of anisotropic piezoelectric strain actuators to control wing deformations, enhancing stability and load alleviation [5]. Morphing technologies such as seamless and active morphing wings have also evolved to advance load control [6, 7]. The research conducted by B.K. Stanford has made significant contributions to the fields of maneuver and gust load alleviation, as well as flutter suppression, through the development of various innovative control surface designs such as the distributed multiple control surfaces. These contributions have been documented in several publications, including [8–11]. Additionally, other recent innovations include the folding wing tip mechanism [12, 13], active winglets, fluidic actuators, and shape memory alloys for load alleviation [14–17].

In contrast, passive load alleviation techniques have gained increasing attention in recent years as alternatives to active methods, offering simplicity and reliability. The integration of composite materials into aircraft structures allows for aeroelastic tailoring, which directs stiffness to control aeroelastic deformations beneficially. Initially introduced by Munk [18] for wooden propellers, this concept has been applied to aircraft wings, particularly for passive load alleviation by controlling material bend-twist coupling to redistribute loads towards the wing root [19–24]. Innovative techniques involving nonlinear structures operating in the post-buckling regime have been explored by Kuder et al. [25] and Hahn et al. [26], showing potential for load alleviation albeit with concerns about robustness and the impact on aerodynamic performance.

As previously stated, the necessity for substantial control authority in active MLA and the conflict between passive MLA and control authority in aeroelastic tailoring have prompted a substantial body of research on the post-control reversal regime. These developments have been driven by the theoretical proof that post-control surface reversal operations offer a significantly higher degree of control authority [27]. Initiatives such as the Active Aeroelastic Wing program have demonstrated the potential for control surfaces to be used in their reversed mode for enhanced maneuverability in military aircraft, rather than solely for load alleviation. This is exemplified by the modified F/A-18 X-53, as cited in [28]. Building on these studies, White et al. [29] investigated novel control effectors, such as variable sweep-raked wing tips, intending to enhance aileron reversal for improved maneuverability. Further investigations by Li et al. [30] analyzed post-control surface reversal behavior, while Griffin and Chen proposed adaptive solutions such as Variable Stiffness Spar for maintaining control authority in both pre- and post-reversal regimes. In a recent publication, Sharpe et al. [31] proposed a novel concept, termed ”tailerons,” which are devices that enable instantaneous operation in reverse mode and act as divergence and flutter suppression mechanisms. The concept was demonstrated in the Dawn One solar aircraft, where it was found to offer promising weight savings and performance enhancements in low-wing-loading aircraft.

It is evident, that there is a notable absence in the existing literature of research investigating the potential for enhancing the load alleviation capabilities of commercial aircraft through the utilization of control surfaces operating in reversed mode. Consequently, as part of the *"**Hy**brid load alleviation by fluidic/reversed **Co**ntrol and **No**nlinear **S**tructures (HyCoNoS)"* project within the *"Sustainable and Energy Efficient Aviation (SE^2A)"* Cluster of Excellence, this study delves into the application of aeroelastic tailoring to enable operation in the post-control surface reversal regime. Operating in this regime is theoretically advantageous, as it significantly enhances control effectiveness by inducing substantial torsional deformation in the wing [27, 32]. The objective of the presented research is to exploit this phenomenon by tailoring the aeroelastic response to facilitate control surface reversal, thereby maximizing load alleviation capabilities while taking into account structural and aeroelastic constraints.

To conclude, this paper is structured as follows. Section 2 details the methodology, describing PROTEUS and the necessary modifications to study control surface reversal and apply active MLA. Section 3 introduces the reference configuration and design studies aimed at maximizing negative aileron effectiveness and minimizing the primary structural mass through active MLA with conventional and reversed control. Finally, Section 4 analyzes the results, and Section 5 presents the conclusions and outlines the future work.

2 MODELLING APPROACH

The model used in this thesis is based on PROTEUS, a framework for aeroelastic analysis and optimization of composite wings developed at TU Delft, initially by the work of De Breuker [33] and extended by the work of Werter [2]. The framework is modified to fulfill the optimization cases and to apply active MLA.

2.1 PROTEUS Framework

Figure 1 provides a visual representation of the PROTEUS framework, which initiates with the optimization procedure. This stage includes defining the wing properties and load cases. The properties cover the planform geometry and airfoils for each section, structural layout specifying the number and position of spars, rib spacing, and stringer spacing-material properties, and the equivalent properties of the stringers. Additionally, if necessary, non-structural masses such as engines and fuel tanks can be specified and adjusted for the analysis of different flight conditions. Load cases are established based on load factor, flight conditions, and fuel mass distribution, and remain constant throughout the optimization process.

Once the inputs have been defined, the wing structure is divided into discrete laminate regions. These regions possess distinct laminate properties, which are specific to the various components of the wing box, such as the upper and lower skins, front and rear spars, and so on. These laminate regions constitute the design area of the optimization problem. The properties (stacking sequence and ply angles) of each laminate are transformed into lamination parameters (LPs), which provide a continuous representation of the laminate's stiffness properties. This is suitable for the implementation of efficient gradient-based optimization algorithms. The description of each laminate is completed by specifying the corresponding thickness, thus comprising nine Design Variables (DVs): eight LPs and one thickness. Furthermore, the cross-sectional modeler developed by Ferede and Abdalla [34] is employed to condense the three-dimensional geometry into equivalent Timoshenko stiffness matrices for each finite element, utilizing the laminate properties and the wing geometry. Subsequently, a co-rotational framework, as described by Battini [35], is employed to develop a geometrically non-linear beam model.

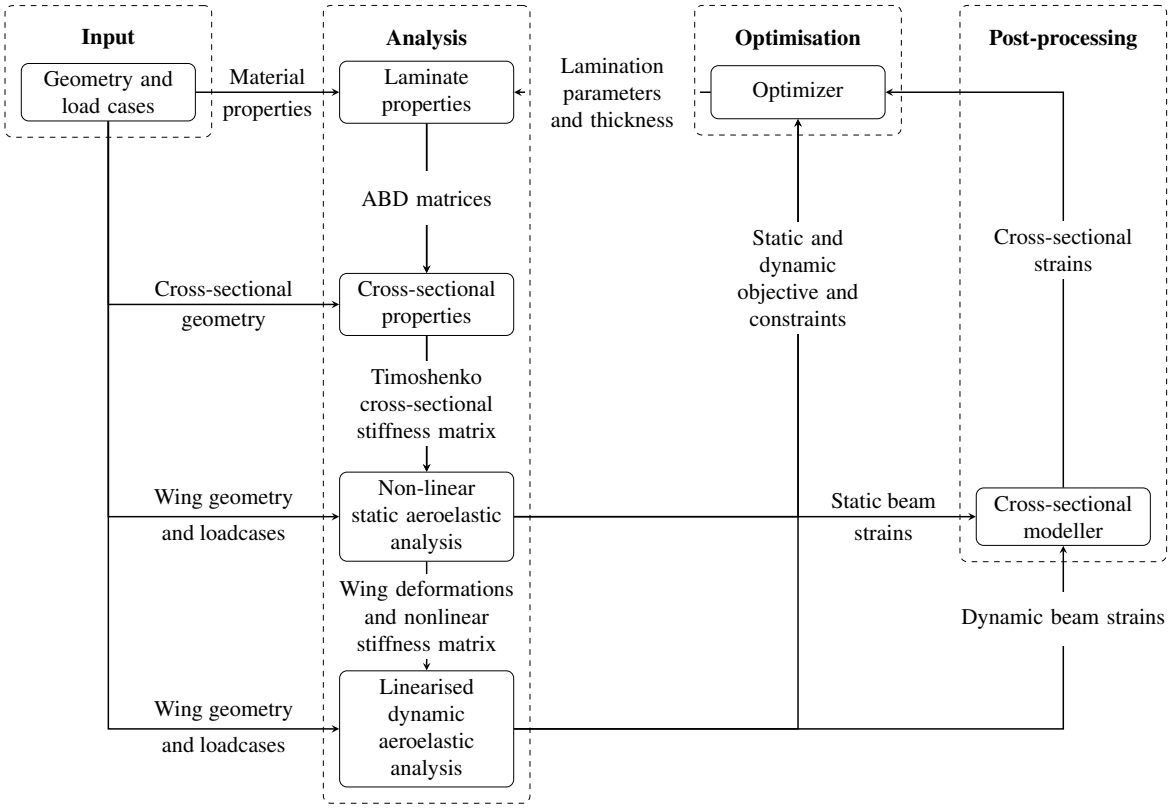

Figure 1: Flowchart of the Proteus framework, adapted from [2].

The geometrically non-linear beam model is then coupled with an aerodynamic model to obtain the aeroelastic model. The aerodynamic model is implemented using the Unsteady Vortex Lattice Method (UVLM), which is a linear model based on potential flow theory [36]. This model assumes a thin wing and discretizes the camber surface into vortex ring elements in both chordwise and spanwise directions. The aerodynamic mesh comprises spanwise-distributed rigid airfoils, each of which is represented by a camber line. The locations of the camber lines are updated under local structural deformations. In this model, the flow is assumed to be inviscid and irrotational, while compressibility effects are considered using the Prandtl–Glauert transformation, which adapts the model for the high subsonic regime. Subsequently, the aerodynamic forces computed for each panel are transferred to the structural beam through a rigid link, and finally, these forces are converted into statically equivalent nodal forces.

The structural and aerodynamic models are monolithically coupled together through a series of coupling matrices, which are extensively explained in the work of Werter [2]. Thus, a dynamic aeroelastic formulation in continuous-time state space form has been developed, describing the dynamic aeroelastic response of a wing to external perturbations. Relying on this approach, aeroelastic stability is evaluated through eigenvalue analysis, and the response to discrete loads is computed. However, in this research, steady analysis will be utilized to calculate maneuver loads, and the unsteady solver will only be used for assessing aeroelastic stability.

In addition, control effectiveness is also calculated to evaluate the control authority in the selected design load cases. The approach implemented in PROTEUS is the one formulated by [21] and is computed as the negative ratio between the rolling coefficient, C_{L_δ}, due to control surface

deflection δ and the rolling coefficient due to roll damping $C_{\mathrm{L_p}}$:

$$n_{\text{ail}} = -\frac{C_{L_\delta}}{C_{L_p}} = \frac{p_{\text{roll}} s}{\delta v_\infty} \tag{2}$$

where p_{roll} represents the steady roll rate for a given control surface deflection; s and v_∞ represent the wing semispan and the airspeed. To compute p_{roll}, an anti-symmetric aerodynamic analysis is performed around the steady symmetric aerodynamic solution, where each positive vortex ring element on the modeled wing has a negative image on the other wing. The flow tangency condition is modified to account for the contribution of the roll motion to the local airflow. The roll rate, p_{roll}, is introduced as an additional degree of freedom, and the roll moment equilibrium is added as an additional equation to the system to be solved.

Furthermore, the assessment of laminate failure utilizes the cross-sectional modeler, recovering the skin strains from the one-dimensional beam strains following the completion of the aeroelastic analysis. Additionally, the in-plane loading is extracted to evaluate the buckling constraint for each buckling panel, which is defined as a patch of laminate delimited by ribs, spars, and stringers. Each panel is approximated as a flat plate with constant stiffness and simply supported boundary conditions on all edges, and is subject to constant in-plane loading. The inverse buckling reserve factor is calculated as the ratio between the applied load and the minimum buckling load.

Finally, after evaluating all objectives, constraints, and their sensitivities with respect to the Design Variables (DVs), they are input into a gradient-based optimizer, the Globally Convergent Method of Moving Asymptotes (GCMMA) [37], to conclude the optimization problem. In summary, Table 1 depicts the capabilities of the PROTEUS framework in its current state.

Table 1: Capabilities of the PROTEUS framework.

Type	**Functionality**
Objectives	Minimum Weight, Maximum Range
Constraints	Strength, Aileron Effectiveness, Buckling, 1g Twist, Blending, Laminate Feasibility
Type of Analysis	Linear or Non-Linear Static Aeroelastic, Linearised Dynamic Aeroelastic
Design Variables	Laminate Properties, Twist Morphing

2.2 Modifications to the Computational Framework

The PROTEUS framework was modified to meet the requirements of this study. The modifications focused on the application of active MLA by deploying the control surfaces in addition to composite tailoring and the management of optimization objectives and constraints.

Active MLA is achieved by deflecting the wing's control surfaces, thereby manipulating the aerodynamic loads acting on the wing. Consequently, the aerodynamic solver of PROTEUS was modified to account for the deflections of the control surfaces and transfer these loads to the structure. Given that the aerodynamic model is based on the Vortex-Lattice Method (VLM), the calculation of the vortex strength distribution on the wing surface is given by the following equation:

$$\mathbf{K}_{\text{st}} \boldsymbol{\Gamma}_{\mathbf{b}} = -\mathbf{V}_\infty \cdot \mathbf{n}_{\mathbf{p}} \tag{3}$$

where, $\mathbf{K}_{\mathrm{st}}$ is the static aerodynamic influence coefficients (AIC) matrix, $\mathbf{\Gamma_b}$ is the vortex strength distribution, $\mathbf{V}_\infty$ is the free-stream velocity and $\mathbf{n_p}$ is the normal vector of the aerodynamic panels. Therefore, there are two possible approaches to account for the deflections of the control surfaces: either by deflecting the aerodynamic mesh in accordance with the deflections of control surfaces or by solely adjusting the boundary conditions of the elements affected by this deflection. In the first option, the AIC matrix must be recalculated for each case. In contrast, in the second option, the AIC matrix is maintained constant, as is the aerodynamic mesh, while the deflections of the control surfaces are implicitly accounted for by superimposing them with the local camber of the configuration without control surface deflections:

$$\mathbf{n}_\mathbf{p}^{MLA} = \mathbf{n_p} + \mathbf{n_{CS}} \tag{4}$$

where $\mathbf{n_{CS}}$ is the normal vector of the aerodynamic panels associated with the control surfaces and $\mathbf{n}_\mathbf{p}^{MLA}$ is the normal vector of the panels of the configuration with active MLA. In the last option, the computing requirements are rather low because the expensive recalculation of the AIC matrix is avoided, and only the system of equations in eq. (3) needs to be solved again. However, this assumption holds for small deflections where the change in the AIC matrix is minimal. Consequently, in order to minimize the computational requirements, the second option was selected.

The primary focus of this study is to enhance the control surface reversal regime as much as possible. Accordingly, the framework must be modified to meet this goal. A viable solution to this problem would be to minimize the dynamic pressure at which reversal onset occurs. However, calculating this with numerical tools is problematic due to the difficulty in deriving analytic derivatives with respect to the DVs. Therefore, an implicit approach to minimize this quantity was chosen: minimizing the control effectiveness at a selected load case, which in turn minimizes the effectiveness at all other flight points and, consequently, the reversal as well.

3 DEFINITION OF DESIGN STUDIES

3.1 Reference Configuration

The selected reference configuration for this study is the Mid-Range (MR) aircraft design developed in the SE^{2}A cluster of excellence, as detailed in [38] and visualized in Figure 12. This MR design is comparable in size and capabilities to the Airbus A320-200. The objective of the design optimization is to achieve a balance between direct operating costs and CO_2-equivalent emissions, which include contrail effects. Consequently, the aircraft design specifies a relatively low and slow operational point at 7650 meters altitude and a Mach number of 0.71. The aircraft is equipped with over-wing engine mounts, an increased wingspan and aspect ratio, and a relatively low wing sweep. Table 2 provides a summary of the aircraft design parameters and masses for the SE^{2}A MR configuration and Table 3 provides an overview of the operating conditions. Further details are available in [38].

As previously noted in [39], the MR aircraft was initially sized using the DLR design process, CPACS-MONA [40], which employed isotropic materials and aircraft flight dynamics. These aspects are beyond the scope of the current study. Consequently, similar to [41], a reference configuration was developed using a conventional mass minimization approach to derive realistic benefit estimates.

The planform geometry, structural layout, movables layout, and non-structural masses are presented on the Figure 2(a). In addition, the structure is divided into five spanwise sections, each

Table 2: Aircraft design parameters and masses.

Parameter	Symbol	Value	Unit
Wing surface	A_{ref}	155.5	m^2
Wingspan	b	43.4	m
Mean aerodynamic chord	c_{MAC}	4.1	m
Wing aspect ratio	Λ	12.11	-
Wing taper ratio	λ	0.26	-
Sweep angle mid-chord	ϕ	12 °	–
Maximum take-off mass	MTOM	65334	kg
Maximum zero-fuel mass	MZM	54964	kg
Operating empty mass	OEM	35313	kg

Table 3: The parameters of the SE^{2}A MR configuration with regard to the flight envelope.

Parameter	Symbol	Value	Unit
Design cruise Mach number	M_c	0.71	-
Maximum operating Mach number	M_{mo}	0.76	-
Maximum operating EAS	v_{mo}	176.5	$\mathrm{m\,s^{-1}}$
Design cruise altitude	H_c	7650	m
Ceiling altitude	H_{max}	11200	m

consisting of laminate regions of equal length. The fuel mass distribution across the span is illustrated in the Figure 2(b). The critical load cases (LCs) used in this study are provided by the project partners and include:

- the cruise condition,
- a pull-up maneuver at sea level, maximum operating speed, and MTOM
- a push-down maneuver at sea level, stall condition, and MTOM
- a pull-up maneuver at design cruise altitude, maximum operating speed, and MZM
- a push-down maneuver at design cruise altitude, stall condition, and MTOM

Further details are presented in Table 4. The selection process was informed by load analysis within the flight envelope. MTOM and ZFM were included in the analysis to account for fuel inertia relief effects.

It is important to note three basic assumptions made in this study. First, rolling maneuvers are not included in the analyzed loads. Depending on the configuration, rolling maneuvers can be critical for the outermost part of the wing, and their omission in the optimization can lead to an overestimation of the wing's flexibility. Second, gust loads are excluded from the analysis due to the high computational cost, which is considered acceptable given the immaturity of the application studied. Finally, critical loads are not updated during the optimization process, which according to [42] could lead to an underestimation of the strength constraints. However, for this application, a deviation of 5% in the stress constraints as stated in [42] is considered acceptable in this study, as the main scope is to fundamentally investigate the impact of aeroelastic tailoring on control effectiveness.

The DVs employed are the same for each optimization study and consist of the LPs and the corresponding laminate thickness per design region. Furthermore, the structure is divided into 5 equally spanned sections as illustrated in Figure 2(a). Each section consists of the front and

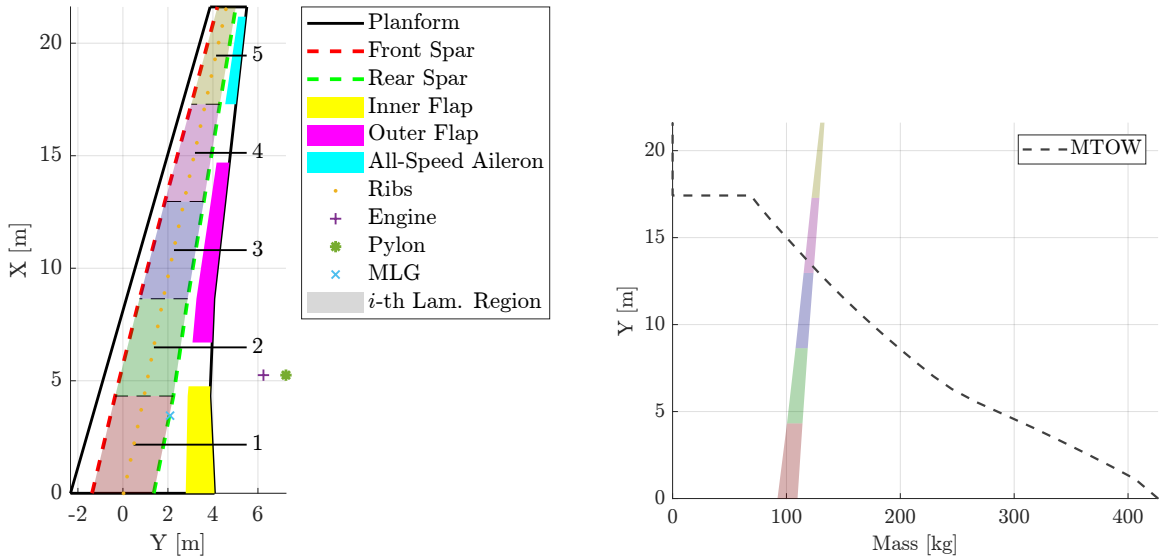

(a) Structural layout, movables layout, non-structural mass distribution, and laminate regions.

(b) Distribution of fuel mass across the wing in MTOW configuration.

Figure 2: Visual representation of the SE^{2}A MR wing.

Table 4: Loadcases utilized in this study.

#LC	Mach Number	Altitude	Mass Case	Load Factor, n_z
1	0.71	7650 m	MTOM	1
2	0.53	0 m	MTOM	2.5
3	0.35	0 m	MTOM	-1
4	0.76	6010 m	ZFM	2.5
5	0.54	6010 m	MTOM	-1

rear spars and the top and bottom skins, so there are four design regions per section. Only symmetric unbalanced laminates are considered, so each laminate is described by eight LPs (four for the A matrix and four for the D matrix) and the thickness. Moreover, in order to consider the jig shape in the optimization studies, the twist angle ϕ_t per element is introduced forming another set of DVs.

Therefore, the total number of DVs is calculated as follows:

$$n_{DV} = n_{\text{section}} \times n_{\text{lam}_{\text{section}}} \times (8\ \text{LPs} + 1\ \text{Thickness} + n_{\phi_t}) = 190 \tag{5}$$

Finally, the material properties used for all optimization cases are presented in Table 5. The following subsections provide detailed information about each study.

Table 5: Single ply material properties.

E_{11}	E_{22}	G_{12}	ν_{12}	Density	Ply thickness
170 GPa	9.9 GPa	5.1 GPa	0.35	1452 kg m^{-3}	0.15 mm

3.2 Negative Control Effectiveness Maximization

To explore the feasibility of aileron control reversal within the flight envelope, various optimization scenarios with different constraint activation were established. The objective was changed

from mass minimization to negative aileron effectiveness maximization for the loadcase describing the cruise conditions, LC 1. These scenarios vary by the set of activated constraints to pinpoint the more critical ones and to gauge the maximum negative control effectiveness achievable. The design variables are consistent with those defined in Section 3.1. Moreover, the most promising design in terms of negative control authority will inform the subsequent mass minimization study that incorporates active MLA with a constraint on negative control effectiveness. Table 6 outlines the nomenclature for these cases and the specific constraints active in each case.

Table 6: Description of control effectiveness minimization cases.

Constraint/Case	**1**	**2**	**3**	**4**	**5**	**6**
Laminate Feasibility	✓	✓	✓	✓	✓	✓
Strain	X	✓	✓	✓	✓	✓
Aeroelastic Stability	X	X	✓	✓	✓	✓
Buckling	X	X	X	✓	✓	✓
Cruise shape	X	X	X	X	✓	✓
Blending	X	X	X	X	X	✓

Initially, case 1 is established to explore the maximum negative control effectiveness achievable while ensuring the manufacturability of composite laminates. The introduction of strain and buckling constraints in cases 2 and 3 provides insights into failure-related effects when negative control effectiveness is pursued. Furthermore, the incorporation of aeroelastic stability constraints in case 4 examines the critical impact of the high torsional flexibility on the stability of the wing. The cruise shape constraint, added in case 5, preserves aerodynamic performance and explores the technology's feasibility in terms of cruise performance. Finally, case 6 provides insight into the effects of manufacturing on the overall structure.

3.3 Mass Minimization

To investigate the load alleviation potential of a configuration with a control surface in reversed mode, it is first necessary to establish a conventional reference configuration. This configuration is optimized for mass using PROTEUS in order to maintain compatibility and prevent overestimation of the benefits. Consequently, two different optimization studies were conducted: one without considering active MLA and another that takes active MLA into account. The constraints applied in these studies are detailed in Table 7 and remain consistent across both. The deflections of the control surfaces per load case are listed in Table 8. The selected deflections, which were maintained throughout the optimization process, were chosen to be conservative in order to ensure that roll maneuvers could potentially be performed in conjunction with the active MLA function.

In these studies, the minimum thickness of each laminate was constrained to $3\ \mathrm{mm}$ to account for handling qualities during manufacturing, and the maximum thickness was set to $50\ \mathrm{mm}$ to preserve the available design space. Additionally, to ensure adequate control authority, the control effectiveness of the aileron was constrained such that $\eta_{ail} \geq 0.15$, which is equivalent to $1.22^{\circ}\,\mathrm{s}^{-1}$ per degree of aileron deflection.

Furthermore, a similar case was set up where the aileron effectiveness constraint was set to $\eta_{ail} \leq -0.15$ for LC 4, which is located in a region of high dynamic pressure within the flight envelope where control reversal is possible while load cases 1, 2, 3, and 5 were not constrained

Table 7: The constraints of the mass minimization problem.

# Set	Type	Description	Amount
1	Laminate Thickness	Minimum and Maximum	2 per laminate
2	Laminate Feasibility	Feasible region of LPs [43]	6 per laminate
3	Strain	Tsai-Wu failure index [44]	8 per laminate and LC
4	Aeroelastic Stability	Eigenvalue analysis	10 eigenvalues per LC
5	Buckling	Buckling analysis of panels	8 per panel and LC
6	Cruise shape	Ensures cruise performance	2 per element
7	Blending	Structural continuity [45]	4 per laminate
8	Aileron Effectiveness	Based on [21]	1 per LC

Table 8: Control surface deflections for active MLA.

# LC	Inner Flap	Outer Flap	All-Speed Aileron
1	0 °	0 °	0 °
2	15 °	10 °	-15 °
3	-15 °	-10 °	15 °
4	15 °	10 °	-15 °
5	-15 °	-10 °	15 °

at all in terms of control effectiveness. This approach forces the optimizer to consider regions of the design space where the aileron operates in a reversed mode in parts of the flight envelope while minimizing structural mass. Consequently, the roll control authority is likely to be diminished in a significant part of the flight envelope, contrary to certification specifications [46]. Nevertheless, this issue is currently being disregarded to focus on the feasibility of this application. Depending on the results, the preservation of control authority in the critical parts of the flight envelope will be addressed in future research.

4 RESULTS

This section presents the results of negative aileron control effectiveness maximization and mass minimization with and without active MLA. Due to the large number of cases focusing on the maximization of negative aileron effectiveness, only the most significant results will be detailed.

The resulting structural designs are examined using two methods. Firstly, the visualization of the in-plane and out-of-plane stiffness distribution, as introduced by [21], will be utilized for each laminate along with its thickness. Secondly, the stiffness properties of the wingbox are extracted based on the cross-sectional stiffness matrix, C, which relates the cross-sectional strains and curvatures to forces and moments for each element:

$$(F_1, F_2, F_3, M_1, M_2, M_3)^T = C \cdot (\varepsilon_{11}, \varepsilon_{12}, \varepsilon_{13}, \kappa_1, \kappa_2, \kappa_3)^T \tag{6}$$

Consequently, the bending stiffness EI, torsional stiffness GJ, bend-twist coupling K, bend-twist coupling factor Ψ, and shear center e with respect to the beam's reference axis are calcu-

lated as follows:

$$\begin{aligned} EI &= C_{55}, \\ GJ &= C_{44}, \\ K &= -C_{45}, \\ e &= -C_{34}^{-1}/C_{44}^{-1}, \\ \Psi &= \sqrt{\frac{K^2}{EIGJ}}. \end{aligned} \tag{7}$$

4.1 Mass Minimization of the Baseline Configuration

The baseline configuration was optimized for minimum mass with and without active MLA. The resulting thickness and stiffness distribution are presented in the appendix, in Figure 13. The discussion of the baseline configuration will not delve into details here, as it is a product of a regular mass minimization case with PROTEUS that has been established in the work of [2]. Nonetheless, it is worthwhile to investigate the effects of active MLA on the structure. As illustrated in Figure 13(b), the optimizer utilizes the thickness of the spars to modify the aeroelastic response. In all the design regions except for the fifth, the rear spar is thicker than the front, thereby shifting the shear center backward to maximize the aileron effectiveness while keeping the structural mass low. The in-plane stiffness is directed towards the trailing edge of the wing to enhance effectiveness. This phenomenon is explained by the principle that directing the in-plane stiffness aft translates to a higher positive bend-twist coupling. This coupling is exploited by the control surfaces, as their downward deflection causes the wing to bend upwards, introducing a nose-up torsional deformation that enhances the lift increment. By doing so, the optimizer maximizes the load alleviation capability of the aileron, shifting as much lift as possible towards the root as shown in Figure 3. Consequently, the thickness of the wing skins is drastically reduced in all design regions, thus reducing the mass by 4% as presented in Table 9.

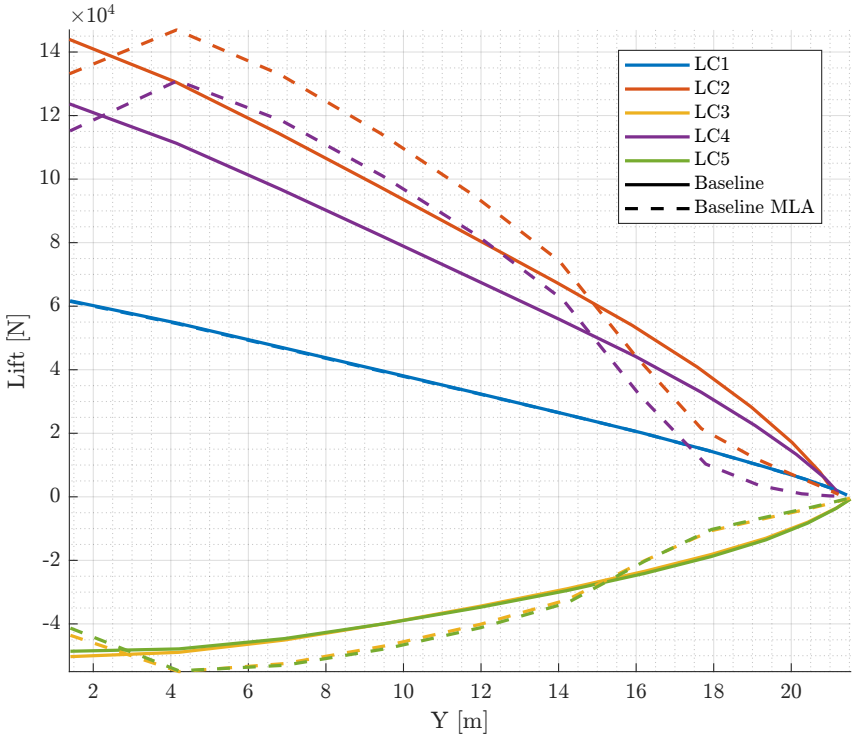

Figure 3: Lift distribution for the baseline configuration, with and without active MLA.

Table 9: Comparison of mass and aileron effectiveness for the baseline configuration with and without active MLA.

Case	Mass		Ail. Effectiveness Cruise		Ail. Effectiveness LC 4	
	kg	%	Actual	%	Actual	%
Baseline	1584.4	-	0.162	-	0.150	-
Baseline MLA	1524.3	-4	0.161	-0	0.150	0

4.2 Negative Control Effectiveness Maximization

This section of the study examines the utilization of aeroelastic tailoring to maximize the negative control effectiveness of the outer aileron. The cases described in Table 6 are analyzed, and the optimized structural designs for each case are illustrated in Figure 14. The resulting mass and control effectiveness in load cases LC 1 and LC 4 are presented in Table 10 and compared to the baseline configuration. These load cases were selected for their representativeness among the analyzed scenarios as LC 1 corresponds to the cruise condition, while LC 4 represents the condition with the highest dynamic pressure, where maximum negative control effectiveness is expected.

Table 10: A comparison of the mass and aileron control effectiveness of the optimization cases is presented. The percentage deviation with respect to the baseline configuration is also calculated.

Case	Mass		Ail. Effectiveness LC 1		Ail. Effectiveness LC 4	
	kg	%	Actual	%	Actual	%
1	1404.5	-11	-0.237	49	-0.382	159
2	1403.8	-11	-0.129	-18	-0.219	49
3	1309.3	-17	-0.106	-33	-0.182	23
4	1498.2	-5	-0.081	-49	-0.154	5
5	2050.9	29	0.004	-98	-0.061	-59
6	2009.6	27	0.000	-100	-0.065	-56

Firstly, in case 1, the potential of composite tailoring is exploited. As illustrated in Figure 4, the principal direction of the in-plane stiffness along a panel, denoted by ϕ_p^A, is defined as the direction of positive rotation around the z-axis (vertical axis). The y-axis runs parallel to the leading edge (LE). In both cases, the principal in-plane stiffness is oriented at a direction

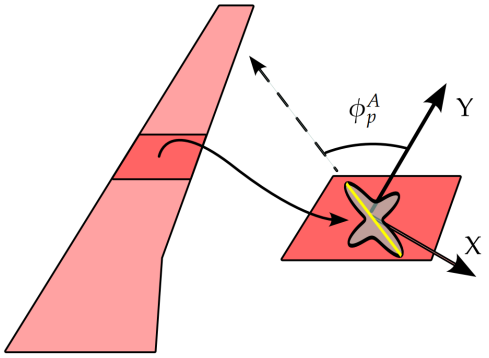

Figure 4: Reference system for defining the principal stiffness direction. The principal stiffness direction with angle ϕ_p^A is represented by the yellow line, while the black curve represents the stiffness rosette.

between 5°-12°, which was demonstrated to maximize the negative bend-twist coupling factor and thus minimize control effectiveness. This effect is also validated by extending the work done in [19] to include the effects of sweep angle as well. The resulting visualization of aileron

effectiveness as a function of sweep angle, ply angle, and airspeed is shown in Figure 5. In these cases, the aileron effectiveness is pushed to extremely higher magnitudes up to 0.382 which is 159% more than the conventional configuration, thus proving the extreme controllability of such structural designs. It is important to note that the optimizer reaches the minimum thickness of $3\mathrm{mm}$ at most of the design regions indicating that the resulting negative control effectiveness could be further decreased by reducing the minimum thickness.

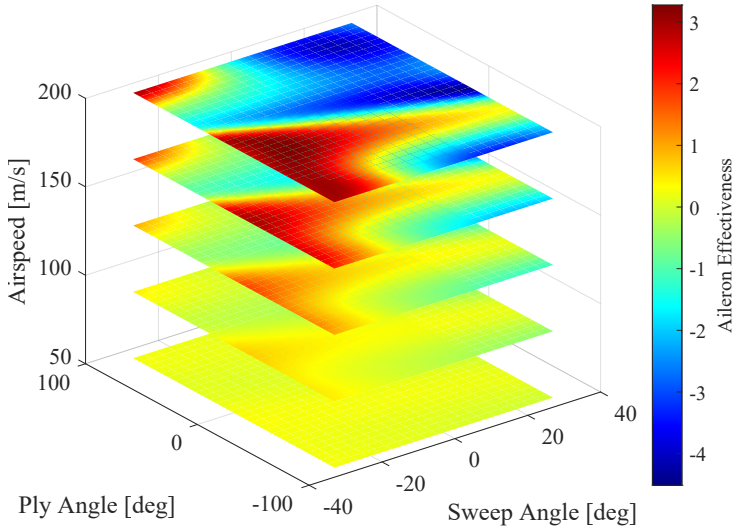

Figure 5: Control effectiveness of the configuration cited in [19]. This study has been extended to account for various sweep angles.

The introduction of the strength constraint in case 2 led to a notable reduction in the margin of the optimization, accompanied by a corresponding reduction in negative control effectiveness, particularly in LC 1, the cruise condition, which is situated within a region of the flight envelope where dynamic pressure is relatively low. This was a consequence of the thickness increase at most parts of the structure, which led to lower strains that limit the utilization of the extension-shear coupling mechanism, as evidenced by the visualization of the in-plane stiffness in Figure 14(b). In contrast, the negative effectiveness of the aileron for LC 4 was found to be satisfactory, approaching the effectiveness of the baseline structure. It is, however, important to note that by considering multiple chordwise design regions and more spanwise design regions, the optimizer could potentially eliminate excess thickness in regions where it was not necessary, thus increasing flexibility and increasing the negative control effectiveness.

The incorporation of aeroelastic stability significantly impacted control effectiveness at both LC 1 and LC 4. In case 2, where the initial configuration highly favored negative control effectiveness, the excessively reduced torsional and bending stiffness was increased as shown in Figure 6. This adjustment compromised the absolute control effectiveness to a 23% increase in comparison to the baseline structure. Additionally, the design exploited the increased thickness of the spars to shift the shear center rearwards and reduce the wash-out effect, thereby enhancing dynamic stability.

The introduction of the buckling constraint in case 4 did not result in any significant alterations to the observed trends, as the in-plane stiffness of the majority of the laminates remained consistent as well as the thickness distribution at a significant portion of the wing structure. However, the buckling constraint became critical for most of the laminates during the optimization process. To mitigate this critical impact, the optimizer employed composite tailoring. One

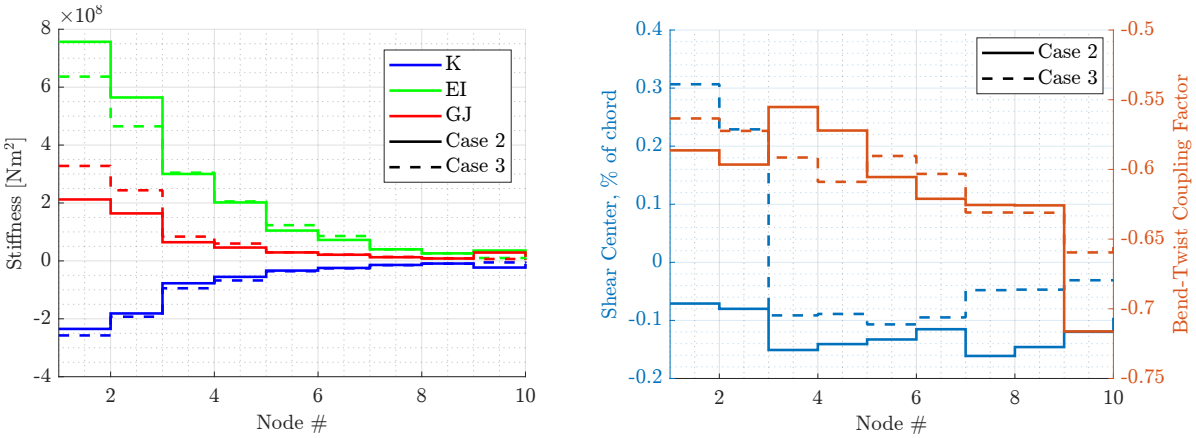

Figure 6: Comparison of stiffness properties of Case 2 and 3

method for mitigating the influence of the buckling constraint is to incorporate cross-ply laminates, which is evident in most of the laminates, as indicated by the star-like bending stiffness visualization depicted in Figure 14(d).

The cruise shape constraint of the SE^{2}A mid-range configuration is presented in Figure 7. As a way to satisfy this constraint, the optimizer employs two mechanisms: first, the adjustment of the jig-twist via the twist morphing variables; and second, the stiffness properties of the wing. In order to minimize the effectiveness of the ailerons, the optimizer should introduce negative bend-twist coupling. The quantity of bend-twist coupling that may be incorporated is dependent on several factors, including the constraints applied to the magnitude of the jig-twist, which are implemented to prevent diminished performance in non-cruise conditions.

The introduction of the cruise shape constraint has a significant impact on case 5. The optimizer is permitted to utilize the negative bend-twist coupling of the wing to a certain extent in order to maximize the negative aileron control effectiveness, as illustrated in Figure 8. However, the restriction to comply with the cruise shape constraint introduces a high wash-in into the jig shape, as shown in Figure 7, in order to counteract the wash-out deformation that arises when cruise loads are applied due to the negative bend-twist coupling. The high wash-in built into the jig shape results in higher wash-in when negative load cases are applied due to the negative bend-twist coupling. Therefore, the amount of negative bend-twist coupling is implicitly limited by the failure-related constraints on the negative load cases, which in turn limits the objective of post-control surface reversal regime enhancement. The overall stiffer design results in limited passive load alleviation capabilities, as illustrated in Figure 9. This, in turn, leads to an increase in the mass of the structure by 29%.

It is important to note that while maintaining the cruise shape is crucial for optimal performance in normal flight conditions, the use of highly effective control surfaces can potentially address this issue by ensuring a constant actuation in a predefined manner. This approach ensures that the cruise shape constraint is satisfied, and consequently, the optimization problem could be redefined, with the deflections at the cruise condition imposed as design variables. Nevertheless, it is also crucial to assess the contribution of the cruise shape constraint to the overall aircraft efficiency. In this case, where high torsional flexibility is desired, the benefits of the structural mass reduction could be higher than that of preserving the optimum aerodynamic shape. Therefore, a better balance between the structural design and aerodynamics could be found. Consequently, simultaneous aerostructural optimization should be performed at the cruise condition.

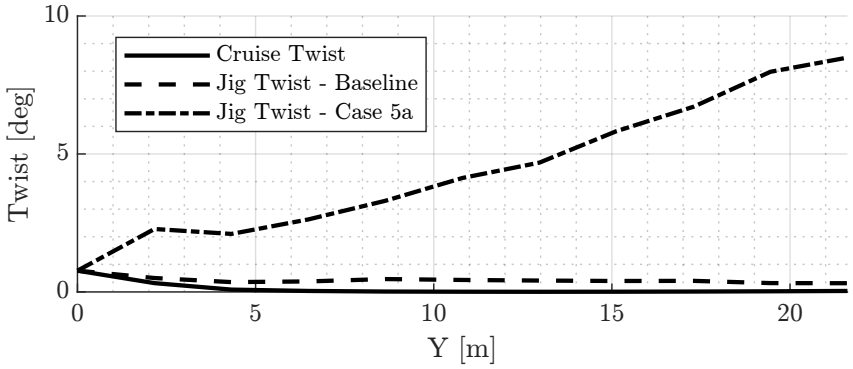

Figure 7: Jig twist comparison of the baseline case and the 5 case along with the cruise twist.

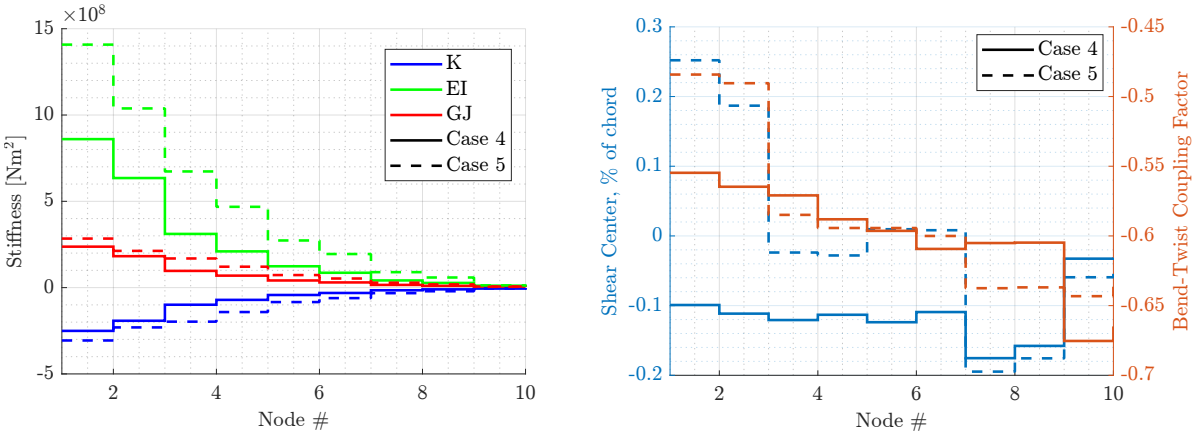

Figure 8: Comparison of stiffness properties of cases 4 and 5.

The introduction of blending constraints effectively constrains the variation in structural properties between different sections. This phenomenon can be observed in Figure 14(f) and is also mentioned in [47]. Consequently, the negative bend-twist coupling of the wing is less effectively exploited, which compromises the negative control effectiveness.

To summarize, it is important to note that although the observed magnitude of aileron control effectiveness is comparable to the baseline case, which includes conventional control surface operation, the results are still encouraging. The reason behind this is the absence of active MLA. The higher controllability of these control surfaces combined with active MLA could reduce the structural stiffness and thus introduce higher negative aileron effectiveness, which increases the load alleviation capabilities. This loop continues until other constraints become active. In contrast, conventional active MLA is unable to leverage this mechanism, as there is an inherent trade-off between controllability and structural stiffness. This concept will be further explored in the subsequent optimization study, which employs an aileron operating in reversed control regime in a mass minimization study with active MLA.

4.3 Active MLA with Reversible Control Surface

In this optimization study, the all-speed aileron was configured to operate in reverse mode, while other movable devices on the aircraft functioned conventionally. A specific constraint was applied to the all-speed aileron, ensuring that $\eta_{ail} \leq -0.15$. Notably, the cruise twist constraint was deactivated to fully leverage the control reversal regime, as the previous findings have shown that this constraint significantly obstructs achieving this objective. The results, which detail both mass and control effectiveness, are presented in Table 11. The data indicate a 15%

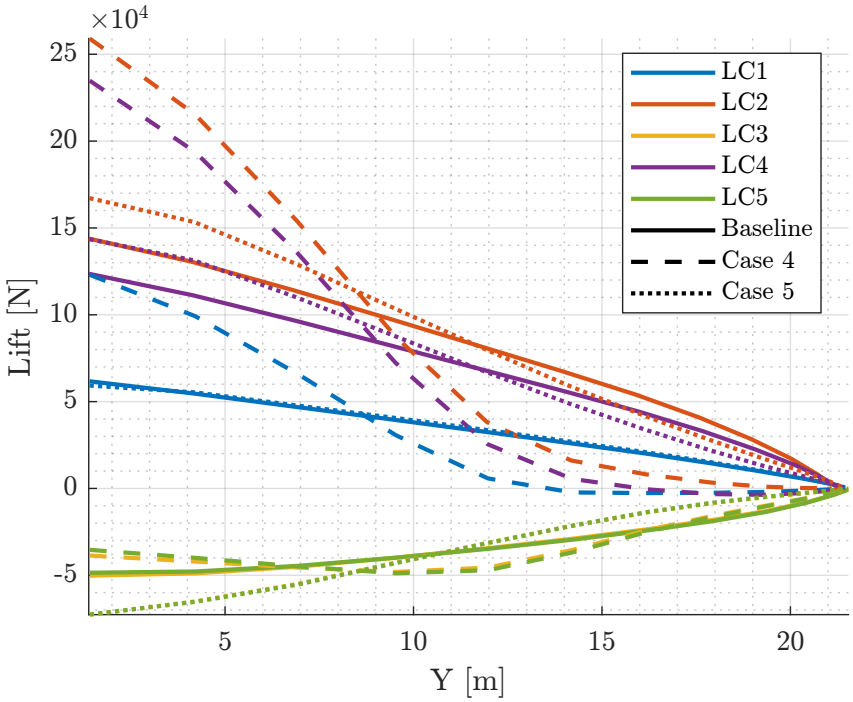

Figure 9: Lift distribution comparison of cases 4 and 5 along with the baseline structure.

and 11% reduction in mass, respectively, in comparison to the baseline case and the conventional active MLA. However, the control effectiveness in LC 1 decreased by 49%, highlighting a major limitation of this study. Future efforts will focus on addressing this issue.

Table 11: Comparison of mass and aileron effectiveness between the case with inverted aileron and conventional cases.

Case	**Mass**		**Ail. Effectiveness Cruise**		**Ail. Effectiveness LC 4**	
	kg	%	Actual	%	Actual	%
Baseline	1584.4	-	0.162	-	0.150	-
Conventional MLA	1524.3	-4	0.161	-0	0.150	0
Inverted MLA	1346.0	-15	-0.081	-49	-0.150	0

The distribution of thickness and stiffness is depicted in Figure 13(c). It is apparent that the thickness of the laminates across a significant portion of the wing was minimized to the lowest feasible limit of 3 mm, due to the load redistribution towards the wing's root while the stiffness patterns exhibited a pronounced tendency to facilitate control reversal. Consequently, both the mass reduction and the increase in negative control effectiveness were limited. As a result, an opportunity for further mass reduction could be explored by lowering the minimum thickness. Conversely, the design region near the root saw a moderate decrease in thickness due to the load redistribution. The bottom skin thickness remained unchanged or increased in some areas to counteract reduced load alleviation capabilities, particularly in negative load factor scenarios that typically govern bottom skin sizing due to buckling. In LC 3 and LC 5, a significant part of the bottom skin exhibited severe buckling factors that approximated a factor of 1, as illustrated in Figure 11. This resulted in a moderate thickness reduction. The thickness reduction compared to the conventional active MLA case is depicted in Figure 10.

The findings of this study indicate that the utilization of the post-control surface reversal regime

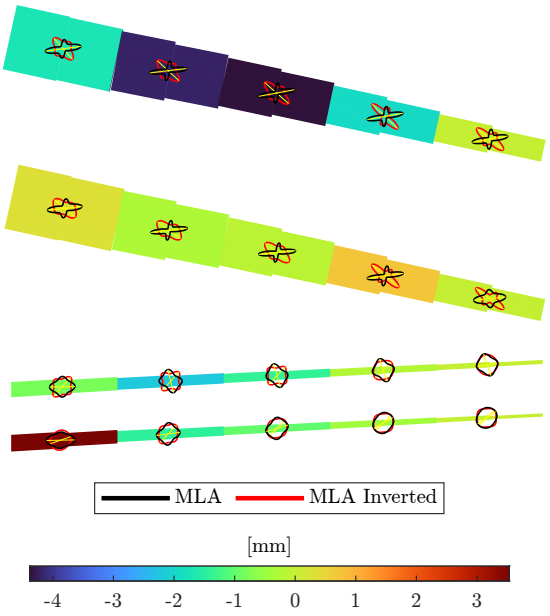

Figure 10: Comparison of thicknesses and in-plane stiffness for cases with conventional active MLA and active MLA with reversible aileron. Components are displayed in a vertical sequence: upper skin, lower skin, front spar, and rear spar, from top to bottom.

of an all-speed aileron has the potential to result in substantial mass reductions. The use of thinner laminates could be employed to further decrease the stiffness, thereby enhancing the negative control effectiveness and increasing the mass savings. The initial hypothesis that operating in reverse mode could significantly improve the load alleviation potential is validated. However, the results are potentially optimistic due to the absence of the cruise shape constraint. Therefore, future work should address this issue.

5 CONCLUSIONS

This study illuminates the potential of aeroelastic tailoring to enhance the post-control surface reversal regime for the outer aileron of the SE^2 mid-range aircraft. A systematic investigation of aeroelastic constraints revealed their critical role in maximizing negative aileron effectiveness and identified key constraints that could become enablers for future designs. Despite the incorporation of failure, aeroelastic stability, and manufacturing constraints limiting the post-control surface reversal regime, the control effectiveness achieved was equivalent to that of conventional structures. Furthermore, the structural mass of the wing was reduced by 5%. However, the cruise twist constraint was notably severe, limiting the negative control effectiveness to unacceptable levels due to its restriction on the redistribution of aerodynamic loads towards the wing root. This, in turn, stiffened the wing and reduced its passive load alleviation capabilities.

Despite these limitations, the effectiveness of an aileron operating in reversed mode for active MLA was demonstrated through an optimization case with inverted aileron deflections which proved superior to conventional structural designs by avoiding the trade-off between flexibility and mass reduction typically caused by load redistribution-induced thickness reduction. The structural mass reductions were substantial, 15% and 11% compared to the baseline and conventional active MLA structural designs respectively, although these results were conservative given the high minimum laminate thickness constraint. Further mass reductions could potentially be achieved by increasing negative aileron effectiveness through reduced torsional stiffness, although significant portions of the flight envelope showed diminished aileron effective-

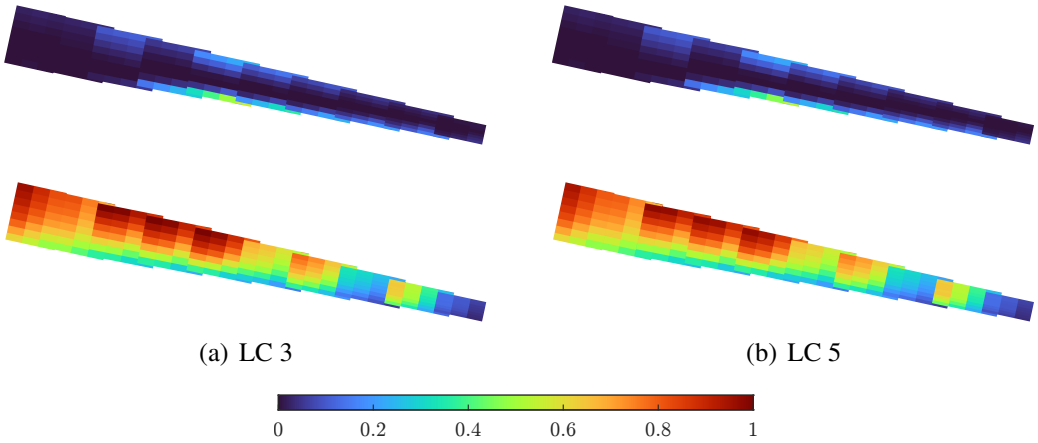

(a) LC 3 (b) LC 5

Figure 11: Buckling factor of the configuration with reversible aileron for all the load cases LC 3 and LC 5. Components are displayed in a vertical sequence: upper and lower skin, from top to bottom.

ness, indicating the need for additional control effectors.

The concept under investigation has the potential to reduce the weight of the wing's primary structure; however, its low technology readiness level necessitates further research to assess its applicability in practice. Future work should focus on parameterizing and including the structural layout and planform geometry in the optimization to enhance geometric bend-twist coupling and identify optimal design points for effective post-control surface reversal operation. Furthermore, the integration of algorithms for optimal control allocation and simultaneous optimization of structural and movable layouts is of paramount importance to facilitate extreme load alleviation while maintaining control authority across the entire flight envelope and minimizing mass. A comprehensive evaluation of aerostructural efficiency is also essential, particularly in terms of how maintaining cruise shape affects overall aircraft performance, to enable radical mass reduction while minimizing the impact on aerodynamic performance. This comprehensive approach will facilitate the use of this technology in future aircraft designs, with the potential to revolutionize control surface functionality and efficiency.

6 ACKNOWLEDGEMENTS

We would like to acknowledge the funding by the Deutsche Forschungsgemeinschaft (DFG, German Research Foundation) under Germany´s Excellence Strategy – EXC 2163/1 - Sustainable and Energy Efficient Aviation – Project-ID 390881007.

7 REFERENCES

[1] Binder, S., Wildschek, A., and De Breuker, R. (2021). The interaction between active aeroelastic control and structural tailoring in aeroservoelastic wing design. *Aerospace Science and Technology*, 110, 106516. ISSN 1270-9638. doi:10.1016/j.ast.2021.106516.

[2] Werter, N. (2017). *Aeroelastic Modelling and Design of Aeroelastically Tailored and Morphing Wings*. Ph.D. thesis, Delft University of Technology. doi:10.4233/UUID:74925F40-1EFC-469F-88EE-E871C720047E.

[3] Krüger, W. R., Dillinger, J., De Breuker, R., et al. (2019). Investigations of passive wing technologies for load reduction. *CEAS Aeronautical Journal*, 10(4), 977–993. ISSN 1869-5582, 1869-5590. doi:10.1007/s13272-019-00393-2.

[4] Regan, C. D. and Jutte, C. V. (2012). Survey of Applications of Active Control Technology for Gust Alleviation and New Challenges for Lighter-weight Aircraft. *NASA/TM-2012-216008*.

[5] Cesnik, C., Ortega-Morales, M., and Patil, M. (2000). Active aeroelastic tailoring of high aspect ratio composite wings. In *41st Structures, Structural Dynamics, and Materials Conference and Exhibit*. Atlanta,GA,U.S.A.: American Institute of Aeronautics and Astronautics, p. 1331. doi:10.2514/6.2000-1331.

[6] Wang, X., Mkhoyan, T., Mkhoyan, I., et al. (2021). Seamless Active Morphing Wing Simultaneous Gust and Maneuver Load Alleviation. *Journal of Guidance, Control, and Dynamics*, 44(9), 1649–1662. ISSN 1533-3884. doi:10.2514/1.G005870.

[7] Smith, D. D., Lowenberg, M. H., Jones, D. P., et al. (2014). Computational and Experimental Validation of the Active Morphing Wing. *Journal of Aircraft*, 51(3), 925–937. ISSN 0021-8669, 1533-3868. doi:10.2514/1.C032262.

[8] Stanford, B. (2018). Aeroservoelastic Optimization under Stochastic Gust Constraints. In *2018 Applied Aerodynamics Conference*. Atlanta, Georgia: American Institute of Aeronautics and Astronautics. ISBN 978-1-62410-559-3, p. 2837. doi:10.2514/6.2018-2837.

[9] Stanford, B. (2020). Optimal Aircraft Control Surface Layouts for Maneuver and Gust Load Alleviation. In *AIAA Scitech 2020 Forum*. Orlando, FL: American Institute of Aeronautics and Astronautics. ISBN 978-1-62410-595-1, p. 0448. doi:10.2514/6.2020-0448.

[10] Stanford, B. K. (2016). Optimization of an Aeroservoelastic Wing with Distributed Multiple Control Surfaces. *Journal of Aircraft*, 53(4), 1131–1144. ISSN 0021-8669, 1533-3868. doi:10.2514/1.C033613.

[11] Stanford, B. K. (2016). Static and Dynamic Aeroelastic Tailoring with Variable-Camber Control. *Journal of Guidance, Control, and Dynamics*, 39(11), 2522–2534. ISSN 0731-5090. doi:10.2514/1.G000413. Publisher: American Institute of Aeronautics and Astronautics.

[12] Castrichini, A., Hodigere Siddaramaiah, V., Calderon, D. E., et al. (2016). Nonlinear Folding Wing Tips for Gust Loads Alleviation. *Journal of Aircraft*, 53(5), 1391–1399. ISSN 0021-8669, 1533-3868. doi:10.2514/1.C033474.

[13] Carrillo, X., Mertens, C., Sciacchitano, A., et al. (2022). Wing Stiffness and Hinge Release Threshold Effects on Folding Wingtip Gust Load Alleviation. In *AIAA SCITECH 2022 Forum*. San Diego, CA & Virtual: American Institute of Aeronautics and Astronautics. ISBN 978-1-62410-631-6, p. 1559. doi:10.2514/6.2022-1559.

[14] Wildschek, A. (2015). Concurrent Optimization of a Feed-Forward Gust Loads Controller and Minimization of Wing Box Structural Mass on an Aircraft with Active Winglets. In *16th AIAA/ISSMO Multidisciplinary Analysis and Optimization Conference*. Dallas, TX: American Institute of Aeronautics and Astronautics. ISBN 978-1-62410-368-1, p. 2490. doi:10.2514/6.2015-2490.

[15] Khalil, K., Asaro, S., and Bauknecht, A. (2022). Active Flow Control Devices for Wing Load Alleviation. *Journal of Aircraft*, 59(2), 458–473. ISSN 1533-3868. doi:10.2514/1.C036426.

[16] Hosseini, S. S., Van Dam, C. P., and Pandya, S. A. (2019). Aerodynamic Load Control for Multi-Element Airfoils Using Surface-Normal Trailing-Edge Blowing. *Journal of Aircraft*, 56(4), 1668–1676. ISSN 1533-3868. doi:10.2514/1.C035248.

[17] Karakalas, A. A., Manolas, D. I., Machairas, T. T., et al. (2019). Active load alleviation potential of adaptive wind turbine blades using shape memory alloy actuators. *Wind Energy*, 22(5), 620–637. ISSN 1099-1824. doi:10.1002/we.2311.

[18] Munk, M. M. (1952). Laminated propeller.

[19] Weisshaar, T. (1987). Aeroelastic tailoring - Creative uses of unusual materials. In *28th Structures, Structural Dynamics and Materials Conference*, Structures, Structural Dynamics, and Materials and Co-located Conferences. American Institute of Aeronautics and Astronautics, p. 976. doi:10.2514/6.1987-976.

[20] Werter, N. P. M. and De Breuker, R. (2016). A novel dynamic aeroelastic framework for aeroelastic tailoring and structural optimisation. *Composite Structures*, 158, 369–386. ISSN 0263-8223. doi:10.1016/j.compstruct.2016.09.044.

[21] Dillinger, J. (2014). *Static Aeroelastic Optimization of Composite Wings with Variable Stiffness Laminates*. thesis, Delft University of Technology.

[22] Stodieck, O., Cooper, J. E., Weaver, P. M., et al. (2017). Aeroelastic Tailoring of a Representative Wing Box Using Tow-Steered Composites. *AIAA Journal*, 55(4), 1425–1439. ISSN 0001-1452, 1533-385X. doi:10.2514/1.J055364.

[23] Stanford, B., Wieseman, C. D., and Jutte, C. (2015). Aeroelastic Tailoring of Transport Wings Including Transonic Flutter Constraints. In *56th AIAA/ASCE/AHS/ASC Structures, Structural Dynamics, and Materials Conference*. Kissimmee, Florida: American Institute of Aeronautics and Astronautics. ISBN 978-1-62410-342-1, p. 1127. doi:10.2514/6.2015-1127.

[24] Brooks, T. R., Martins, J. R., and Kennedy, G. J. (2019). High-fidelity aerostructural optimization of tow-steered composite wings. *Journal of Fluids and Structures*, 88, 122–147. ISSN 08899746. doi:10.1016/j.jfluidstructs.2019.04.005.

[25] Kuder, I. K., Arrieta, A. F., Rist, M., et al. (2016). Aeroelastic response of a selectively compliant morphing aerofoil featuring integrated variable stiffness bi-stable laminates. *Journal of Intelligent Material Systems and Structures*, 27(14), 1949–1966. ISSN 1045-389X. doi:10.1177/1045389X15620038. Publisher: SAGE Publications Ltd STM.

[26] Hahn, D., Haupt, M., and Heimbs, S. (2022). Passive Load Alleviation by Nonlinear Stiffness of Airfoil Structures. In *AIAA SCITECH 2022 Forum*. American Institute of Aeronautics and Astronautics, p. 0318.

[27] Wright, J. R. and Cooper, J. E. (2014). *Introduction to Aircraft Aeroelasticity and Loads*. Wiley, 1 ed. ISBN 978-1-118-48801-0 978-1-118-70044-0. doi:10.1002/9781118700440.

[28] Perry, B., Cole, S. R., and Miller, G. D. (1995). Summary of an Active Flexible Wing program. *Journal of Aircraft*, 32(1), 10–15. ISSN 0021-8669. doi:10.2514/3.46677. Publisher: American Institute of Aeronautics and Astronautics.

[29] White, E. V., Kapania, R. K., and Joshi, S. (2015). Novel Control Effectors for Truss Braced Wing. Tech. Rep. NASA/CR-2015-218792. NTRS Author Affiliations: Boeing Co., Virginia Polytechnic Inst. and State Univ., NextGen Aeronautics, Inc. NTRS Document ID: 20150017734 NTRS Research Center: Langley Research Center (LaRC).

[30] Li, W.-E. and Hodges, D. (2010). Enhancement of Roll Maneuverability Using Post-Reversal Design. Part I: Nonlinear Analysis. In *51st AIAA/ASME/ASCE/AHS/ASC Structures, Structural Dynamics, and Materials Conference*, Structures, Structural Dynamics, and Materials and Co-located Conferences. American Institute of Aeronautics and Astronautics, p. 2792. doi:10.2514/6.2010-2792.

[31] Sharpe, P., Dewald, A., and Drela, M. (2023). Tailerons for Aeroelastic Stability and Control of Flexible Wings. In *AIAA AVIATION 2023 Forum*. San Diego, CA and Online: American Institute of Aeronautics and Astronautics. ISBN 978-1-62410-704-7, p. 3951. doi:10.2514/6.2023-3951.

[32] Hodges, D. H. and Pierce, G. A. (2011). *Introduction to structural dynamics and aeroelasticity*, vol. 15. cambridge university press. ISBN 1-139-49992-0.

[33] De Breuker, R. (2011). *Energy-based Aeroelastic Analysis and Optimisation of Morphing Wings*. Ph.D. thesis, Delft University of Technology.

[34] Ferede, E. and Abdalla, M. (2014). Cross-sectional modelling of thin-walled composite beams. In *55th AIAA/ASME/ASCE/AHS/ASC Structures, Structural Dynamics, and Materials Conference*. National Harbor, Maryland: American Institute of Aeronautics and Astronautics. ISBN 978-1-62410-314-8, p. 0163. doi:10.2514/6.2014-0163.

[35] Battini, J.-M. and Pacoste, C. (2002). Co-rotational beam elements with warping effects in instability problems. *Computer Methods in Applied Mechanics and Engineering*, 191(17), 1755–1789. ISSN 0045-7825. doi:10.1016/S0045-7825(01)00352-8.

[36] Katz And, J. and Plotkin, A. (2004). Low-Speed Aerodynamics, Second Edition. *Journal of Fluids Engineering*, 126(2), 293–294. ISSN 0098-2202, 1528-901X. doi:10.1115/1.1669432.

[37] Svanberg, K. (2002). A Class of Globally Convergent Optimization Methods Based on Conservative Convex Separable Approximations. *SIAM Journal on Optimization*, 12(2), 555–573. ISSN 1052-6234. doi:10.1137/S1052623499362822. Publisher: Society for Industrial and Applied Mathematics.

[38] Karpuk, S., Radespiel, R., and Elham, A. (2022). Assessment of Future Airframe and Propulsion Technologies on Sustainability of Next-Generation Mid-Range Aircraft. *Aerospace*, 9(5), 279. ISSN 2226-4310. doi:10.3390/aerospace9050279. Number: 5 Publisher: Multidisciplinary Digital Publishing Institute.

[39] Beyer, Y., Cavaliere, D., Bramsiepe, K., et al. (2023). An Aeroelastic Flight Dynamics Model for Gust Load Alleviation of Energy-Efficient Passenger Airplanes. In *AIAA AVIATION 2023 Forum*. San Diego, CA and Online: American Institute of Aeronautics and Astronautics. ISBN 978-1-62410-704-7, p. 4452. doi:10.2514/6.2023-4452.

[40] Klimmek, T., Schulze, M., Abu-Zurayk, M., et al. (2019). cpacs-MONA – An independent and in high fidelity based MDO tasks integrated process for the structural and aeroelastic design for aircraft configurations. In *International Forum on Aeroelasticity and Structural Dynamics 2019, IFASD 2019*. Savannah, GA (USA).

[41] Sodja, J., Werter, N. P. M., and De Breuker, R. (2021). Aeroelastic Demonstrator Wing Design for Maneuver Load Alleviation Under Cruise Shape Constraint. *Journal of Aircraft*, 58(3), 448–466. ISSN 0021-8669. doi:10.2514/1.C035955. Publisher: American Institute of Aeronautics and Astronautics.

[42] Rajpal, D., Gillebaart, E., and De Breuker, R. (2019). Preliminary aeroelastic design of composite wings subjected to critical gust loads. *Aerospace Science and Technology*, 85, 96–112. ISSN 12709638. doi:10.1016/j.ast.2018.11.051.

[43] Raju, G., Wu, Z., and Weaver, P. (2014). On Further Developments of Feasible Region of Lamination Parameters for Symmetric Composite Laminates. In *55th AIAA/ASME/ASCE/AHS/ASC Structures, Structural Dynamics, and Materials Conference*. National Harbor, Maryland: American Institute of Aeronautics and Astronautics. ISBN 978-1-62410-314-8, p. 1374. doi:10.2514/6.2014-1374.

[44] IJsselmuiden, S. T., Abdalla, M. M., and Gürdal, Z. (2012). Implementation of Strength-Based Failure Criteria in the Lamination Parameter Design Space. *AIAA Journal*. doi: 10.2514/1.35565.

[45] Macquart, T., Bordogna, M. T., Lancelot, P., et al. (2016). Derivation and application of blending constraints in lamination parameter space for composite optimisation. *Composite Structures*, 135, 224–235. ISSN 02638223. doi:10.1016/j.compstruct.2015.09.016.

[46] (2023). CS-25 Amendment 28 | EASA.

[47] Bordogna, M. T., Lancelot, P., Bettebghor, D., et al. (2020). Static and dynamic aeroelastic tailoring with composite blending and manoeuvre load alleviation. *Structural and Multidisciplinary Optimization*, 61(5), 2193–2216. ISSN 1615-1488. doi: 10.1007/s00158-019-02446-w.

COPYRIGHT STATEMENT

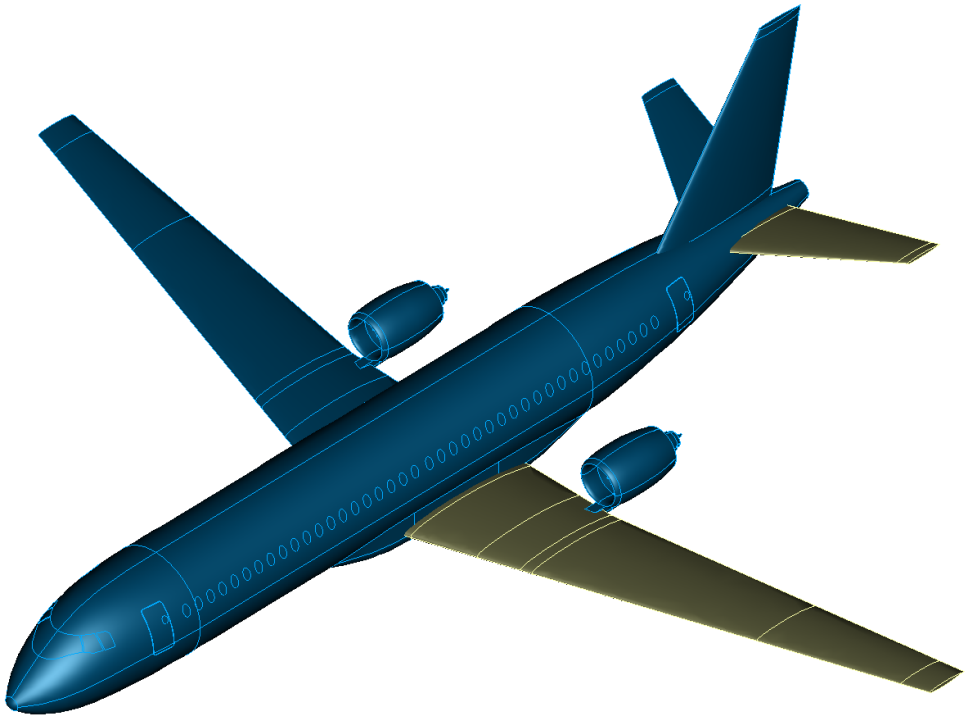

Figure 12: Visualization of SE^{2}A MR aircraft in TiGL

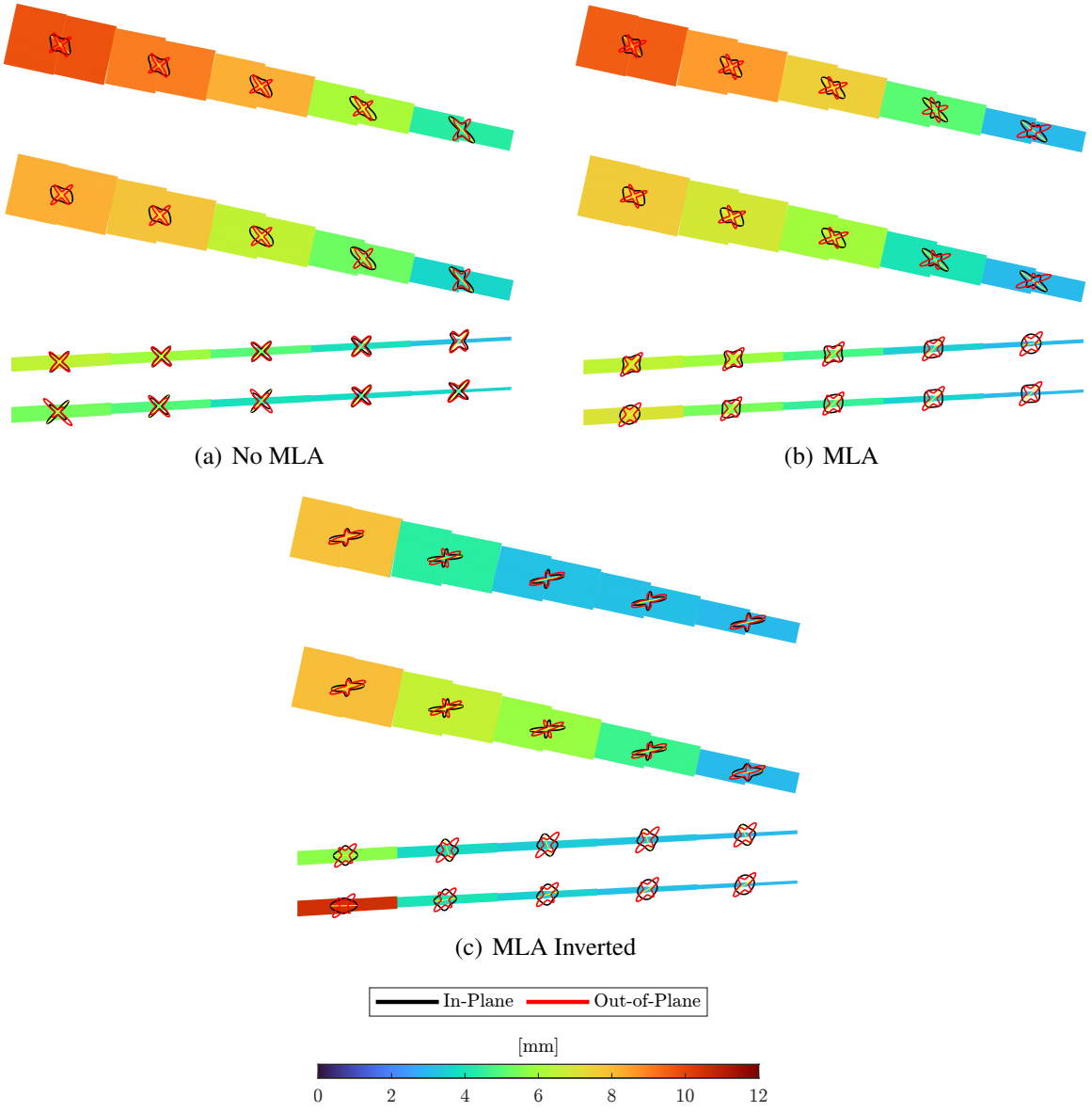

(a) No MLA

(b) MLA

(c) MLA Inverted

Figure 13: Resulting thicknesses and stiffness rosettes of Baseline configuration with active MLA, without active MLA, and active MLA with reversible aileron. Components are displayed in a vertical sequence: upper and lower skin, front and rear spar, from top to bottom.

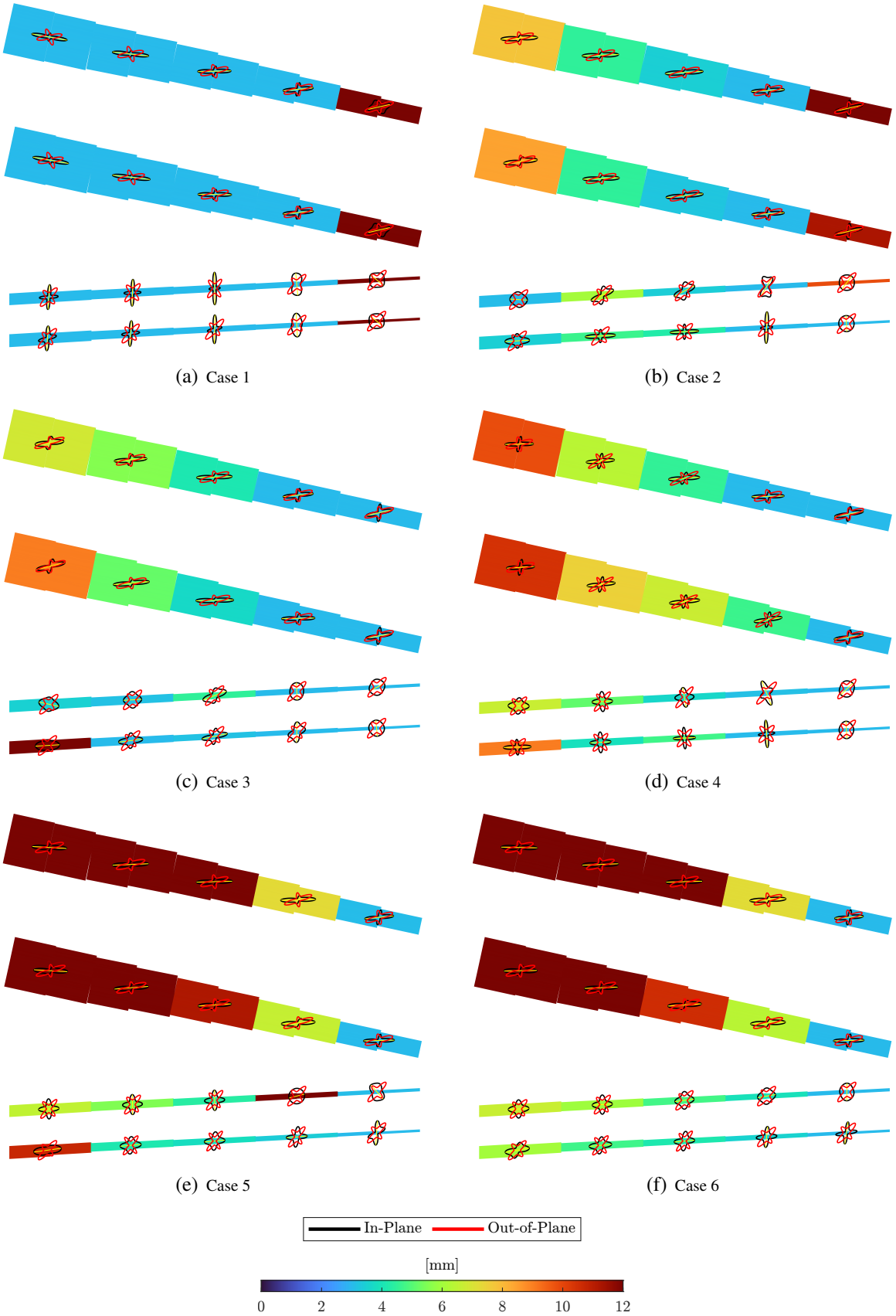

(a) Case 1 (b) Case 2

(c) Case 3 (d) Case 4

(e) Case 5 (f) Case 6

Figure 14: Resulting thicknesses and stiffness rosettes for aileron effectiveness minimization across all cases. Components are displayed in a vertical sequence: upper and lower skin, front and rear spar, from top to bottom.